

Gravitational wave oscillations in Multi-Proca dark energy models

Gabriel Gómez,^a José F. Rodríguez,^{b,c}

^aCentro Multidisciplinario de Física, Vicerrectoría de Investigación, Universidad Mayor, Camino La Pirámide 5750, Huechuraba, 8580745, Santiago, Chile

^bEscuela de Física, Universidad Industrial de Santander, Ciudad Universitaria, Bucaramanga 680002, Colombia

^cICRANet, Piazza della Repubblica 10, 65122, Pescara PE, Italy

E-mail: luis.gomezd@umayor.cl, jose.rodriguez2@correo.uis.edu.co

Abstract. Gravitational wave oscillations arise from the exchange of energy between the metric perturbations and additional tensor modes. This phenomenon can occur even when the extra degrees of freedom consist of a triplet of massive Abelian vector fields, as in Multi-Proca dark energy models. In this work, we study gravitational wave oscillations in this class of models minimally coupled to gravity with a general potential, allowing also for a kinetic coupling between the vector field and dark matter that can, in principle, enhance the modulation of gravitational wave amplitudes. After consistently solving the background dynamics, requiring the model parameters to reproduce a phase of late-time accelerated expansion, we assess the accuracy of commonly used analytical approximations and quantify the impact of gravitational wave amplitude modulation for current detectors (LIGO–Virgo) and future missions such as LISA. Although oscillations are present in these scenarios, we find that the effective mass scale (the mixing mass) governing the phenomenon is $m_g \sim \mu_A$, where μ_A is the (time-dependent) effective mass of the vector dark-energy field. Detectability of gravitational wave oscillations, however, requires $m_g \gg H_0$, which is in tension with the ultra-light masses typically needed to drive accelerated expansion $\mu_A \sim H_0 \sim 10^{-33}$ eV. Therefore, if gravitational wave oscillations were to be detected at the corresponding frequencies, they could not be attributed to these classes of dark-energy models.

Keywords: Gravitational waves, dark energy, vector fields

Contents

1	Introduction	1
2	The model	2
2.1	Background evolution	4
3	Gravitational waves oscillations	7
3.1	Oscillations of the Waveform	8
3.2	A Realistic Scenario	10
4	Conclusions	13
A	Tensor perturbations	14

1 Introduction

In 1918, Einstein predicted the existence of gravitational radiation, in close analogy with electromagnetic waves [1]. Unlike their electromagnetic counterparts, gravitational waves (GWs) interact extremely weakly with matter, making their detection remarkably challenging. The discovery of the Hulse-Taylor binary pulsar [2] provided indirect confirmation of gravitational radiation [3, 4], but it took nearly 100 years to achieve direct detection. The first detection by the LIGO-Virgo collaboration in 2015 [5], an event consistent with a binary black hole merger, marked the beginning of gravitational wave astronomy.

GWs offer a novel probe of fundamental physics and cosmology [6–10]. In particular, they provide an independent means to investigate the nature of dark energy, one of the central open problems in modern cosmology. Historically, the simplest explanation has been the cosmological constant Λ , interpreted as a vacuum energy density [11–13]. However, recent joint analyses combining Baryon Acoustic Oscillation (BAO) measurements from the Dark Energy Spectroscopic Instrument (DESI) Data Release 2 [14], cosmic microwave background (CMB) observations from *Planck* [15], and Type Ia supernova samples [16–18] have provided increasing evidence that the dark energy component may evolve with time at low redshift [19]. These indications add to existing tensions within the standard cosmological model, including the persistent H_0 tension [20, 21] and the long-standing σ_8 tension related to the amplitude of matter fluctuations [22–25].

Motivated by these anomalies, there has been renewed interest in dynamical dark energy scenarios. A well-studied class is provided by scalar-field models, commonly referred to as *quintessence* [26, 27], in which cosmic acceleration is driven by a slowly evolving scalar field rolling along a sufficiently flat potential [28]. Beyond scalar-field descriptions, vector-like dark energy models have also emerged as viable and well-motivated alternatives [29–40]. Among these, a particularly distinctive class is provided by Multi-Proca theories [41–45] (see also Ref. [46] for a generalized and systematic framework including derivative self-interactions). A key feature of vector dark energy models lies in the configuration of the background fields. A single vector field inherently introduces a preferred spatial direction, thereby breaking rotational invariance. In the absence of an internal global symmetry enforcing isotropy, this issue can be circumvented in two main ways: either by considering purely time-like vector

configurations, or by introducing a set of three identical, mutually orthogonal space-like vector fields—commonly referred to as a *cosmic triad* [41].

Since dark energy belongs to a hidden sector, its properties must be probed indirectly, primarily through gravitational interactions. In this context, the advent of GW astronomy opens a new observational window on the dark sector. Early insight into such possibilities dates back to the pioneering work of Gertsenshtein [47], who showed that GWs can convert into electromagnetic waves while propagating through a constant magnetic field. In practice, however, the weakness of this interaction implies that observable conversion would require extremely large propagation distances and coherent magnetic fields, rendering detection unlikely. By contrast, if vector-like dark energy permeates the Universe, analogous mixing effects could be significantly enhanced. This naturally raises the question of whether GW propagation can be exploited as a probe of the fundamental nature of dark energy.

Remarkably, perturbations of Multi-Proca fields also support helicity-2 excitations. These additional tensor modes can couple directly to the metric perturbations, leading to distinctive modifications of GW propagation [48]. Such couplings may arise through friction, velocity, chirality, or mass-mixing terms in the linearized equations of motion [49], altering the dispersion relation and enabling energy exchange between the two sectors. These features are not unique to Multi-Proca fields; they also appear in bigravity models [50, 51].

A general framework for studying GW propagation in the presence of additional tensor degrees of freedom was developed in Refs. [49, 52]. However, those analyses relied on a phenomenological parameterization of the mixing terms, leaving open the question of whether the assumed parameters are compatible with a cosmological background that genuinely produces late-time acceleration. A more self-consistent approach was adopted in Ref. [53], where GW amplitude modulation in the presence of a gauge-field dark energy component was studied alongside the background evolution. That analysis found that, for realistic models, the resulting amplitude oscillations remain far below observational sensitivity.

In this work, we focus on the Multi-Proca dark energy model introduced in Refs. [41, 44] and address the problem in a fully consistent manner. We first solve the cosmological background equations to reproduce the observed expansion history, including late-time acceleration. We then use the resulting background solution to study the coupled evolution of helicity-2 perturbations in both the metric and vector sectors, allowing us to quantify the exchange of energy between them. Our goal is to evaluate the prospects for constraining such scenarios with current and future GW observations.

This paper is organized as follows. In section 2, we present the Multi-Proca model and discuss the background cosmological dynamics. In section 3, we derive the linearized perturbation equations and analyze the implications for GW propagation and observational constraints. Finally, we summarize our findings and outline future directions in section 4.

2 The model

We begin by considering the action of a Multi-Proca theory minimally coupled to gravity, including a general self-interaction potential and a non-trivial coupling to the dark matter sector.¹ The action reads [44]

$$S = \int \left[\frac{M_{\text{Pl}}^2}{2} R - \frac{1}{4} F_{\mu\nu}^a F_a^{\mu\nu} - V(\tilde{X}) + f(X) \mathcal{L}_{\tilde{m}}(g_{\mu\nu}, \psi) \right] \sqrt{-g} d^4x, \quad (2.1)$$

¹Throughout this work we assume that radiation and baryons interact with the Proca fields only through gravity.

where $M_P^2 = (8\pi G)^{-1/2}$ is the reduced Planck mass, R is the Ricci scalar, $F_{\mu\nu}^a \equiv \partial_\mu A_\nu^a - \partial_\nu A_\mu^a$ denotes the field-strength tensor of the vector fields. The function V is a general potential depending on $\tilde{X} \equiv A_{a\mu} A^{a\mu}$, while $\mathcal{L}_{\tilde{m}}(g_{\mu\nu}, \psi)$ represents the Lagrangian of the dark matter field ψ . Finally, $f(X)$ is the coupling function, with $X \equiv -\frac{1}{2} A_{a\mu} A^{a\mu}$.

Varying the action with respect to the metric yields the field equations

$$M_{\text{Pl}}^2 G_{\mu\nu} = T_{\mu\nu} = K_{\mu\nu} + M_{\mu\nu}, \quad (2.2)$$

where $K_{\mu\nu}$ and $M_{\mu\nu}$ denote the contributions of the vector fields and the dark matter sector, respectively, to the total energy-momentum tensor of the Universe. They are defined as

$$K_{\mu\nu} = F_{a\nu\alpha} F_{\mu}^a{}^\alpha - \frac{1}{4} F_{a\alpha\beta} F^{a\alpha\beta} g_{\mu\nu} + 2 A_{a\nu} A_{\mu}^a V_{,\tilde{X}} - V g_{\mu\nu}, \quad (2.3)$$

and

$$M_{\mu\nu} = f \mathcal{M}_{\mu\nu} + f_{,X} \mathcal{L}_{\tilde{m}} A_{a\mu} A_{\nu}^a, \quad (2.4)$$

with,

$$\mathcal{M}_{\mu\nu} = -2 \frac{\partial \mathcal{L}_{\tilde{m}}}{\partial g^{\mu\nu}} + \mathcal{L}_{\tilde{m}} g_{\mu\nu}, \quad (2.5)$$

and $f_{,X}$ denotes differentiation with respect to X . Similarly, variation with respect to the vector fields leads to the Proca equation

$$\nabla_\nu F_{a\mu}^\nu + \mu_A^2 A_{a\mu} = 0, \quad (2.6)$$

where we have introduced the effective mass

$$\mu_A^2 \equiv 2V_{,\tilde{X}} + f_{,X} \mathcal{L}_{\tilde{m}}. \quad (2.7)$$

The second term represents the contribution from the coupling to dark matter, which may be alternatively interpreted as generating an effective dark-matter pressure. Regardless of whether this contribution is viewed as modifying the vector sector or the matter sector, its physical effect is encoded in the combination above.

We consider a homogeneous and isotropic background described by the Friedmann-Lemaitre-Robertson-Walker (FLRW) metric,

$$ds^2 = a^2(\eta) (-d\eta^2 + \delta_{ij} dx^i dx^j), \quad (2.8)$$

written in conformal time, with $d\eta = dt/a$. To preserve the symmetries of the background, we introduce a triad of mutually orthogonal, space-like vector fields with a common norm φ

$$A_\mu^a \equiv \varphi(\eta) \delta_\mu^a. \quad (2.9)$$

Here $a(\eta)$ denotes the scale factor. Varying the action on this background leads to the following field equations:

$$3M_{\text{Pl}}^2 \mathcal{H}^2 = a^2 f \rho_{\tilde{m}} + \frac{3\varphi'^2}{2a^2} + a^2 V = a^2 \rho_T, \quad (2.10)$$

$$M_{\text{Pl}}^2 (\mathcal{H}^2 + 2\mathcal{H}') = -\frac{\varphi'^2}{2a^2} + a^2 V - \mu_A^2 \varphi^2 = -a^2 p_T, \quad (2.11)$$

$$\varphi'' + a^2 \mu_A^2 \varphi = 0, \quad (2.12)$$

where ρ_T and p_T are the total energy density and isotropic pressure associated to both dark fluids, respectively. Here, prime denotes derivatives with respect to the conformal time, $\mathcal{H} \equiv a'/a$ is the conformal Hubble parameter, and $\mathcal{L}_{\tilde{m}} = -\rho_{\tilde{m}}$ corresponds to the cold dark matter Lagrangian density. The energy density and isotropic pressure associated with the vector fields, as measured by a comoving observer, are

$$\rho_A = \frac{3}{2} \frac{\varphi'^2}{a^4} + V, \quad (2.13)$$

$$p_A = \frac{1}{2} \frac{\varphi'^2}{a^4} - V + \mu_A^2 \frac{\varphi^2}{a^2}. \quad (2.14)$$

The corresponding continuity equations follow directly from the Bianchi identities and read

$$\rho'_A + 3\mathcal{H}(\rho_A + P_A) = \frac{3\varphi}{a^2}(\varphi' - \mathcal{H}\varphi)f_{,X}\rho_{\tilde{m}}, \quad (2.15)$$

$$\rho'_{\tilde{m}} + 3\mathcal{H}\rho_{\tilde{m}} = -\frac{3\varphi}{a^2}(\varphi' - \mathcal{H}\varphi)f_{,X}\rho_{\tilde{m}}. \quad (2.16)$$

These equations clearly show that the two components exchange energy through a dynamical interaction mediated by the coupling function. It is worth noticing that the general formulation presented here differs slightly from Ref. [44], which was written in cosmic time, but it is straightforward to verify that both descriptions are fully equivalent.

2.1 Background evolution

To solve for the background dynamics, all quantities are expressed in dimensionless form by normalizing to their present-day values. The set of background equations is written as a first-order system for the variables according to the state vector $\{\psi, \chi, a, \mathcal{H}, \hat{\rho}_m\}$, where the variables $\psi \equiv \varphi/M_{\text{Pl}}$ and $\chi \equiv \psi'$ represent, respectively, the rescaled vector field amplitude and its conformal-time derivative; and $\hat{\mathcal{H}} = \mathcal{H}/H_0$. Setting $a_0 = 1$, leads directly to $\hat{\mathcal{H}}_0 = 1$. All energy densities are normalized to the present critical density as $\hat{\rho}_i = \rho_i/\rho_{\text{crit},0}$, while the conformal time η is expressed in units of H_0^{-1} .

We adopt two common forms for the self-interacting potential: an exponential potential and a power-law potential,

$$\hat{V}_1(\hat{\tilde{X}}) = \hat{V}_{01} e^{-\lambda \hat{\tilde{X}}}, \quad \hat{V}_2(\hat{\tilde{X}}) = \hat{V}_{02} \hat{\tilde{X}}^{-\beta}. \quad (2.17)$$

For the coupling function, we assume a power law coupling

$$f(\hat{X}) = (1 + \alpha \hat{X})^n, \quad (2.18)$$

where $\hat{\tilde{X}} = 3\left(\frac{\psi}{a}\right)^2$ and $\hat{X} = -\frac{3}{2}\left(\frac{\psi}{a}\right)^2$. Here, λ , β and \hat{V}_{0i} are free parameters of the potentials, while α and n are the coupling parameters of the vector field. Since f is a real-valued function, this implies the bound $\left(\frac{\psi}{a}\right)^2 < \frac{2}{3\alpha}$ at all times.

The conditions at the present time are determined consistently from the Friedmann constraint,

$$\hat{\mathcal{H}}^2 = a^2 f \hat{\rho}_m + \frac{1}{2} \left(\frac{\chi}{a}\right)^2 + a^2 \hat{V}(\hat{\tilde{X}}). \quad (2.19)$$

Considering the reference values² $\Omega_{m,0} = 0.32$ and $\Omega_{\text{DE},0} = 0.68$, the scalar field amplitude today is fixed analytically. For the exponential potential, this is constrained to

$$\psi_0 = \sqrt{-\frac{1}{3\lambda} \ln \left(\frac{\Omega_{\text{DE},0} - \chi_0^2/2}{\hat{V}_{01}} \right)}, \quad (2.20)$$

which, in turn, establishes the bound $\hat{V}_{01} \gtrsim \Omega_{\text{DE},0}$ for $\lambda > 0$, or the converse for $\lambda < 0$, provided that the kinetic energy contribution today is very small, as expected. For the power-law potential the constraint reads

$$\psi_0 = \sqrt{\frac{1}{3\beta} \left(\frac{\Omega_{\text{DE},0} - \chi_0^2/2}{\hat{V}_{02}} \right)^{-1/\beta}}. \quad (2.21)$$

As, $\chi_0 \ll 1$, we expect $\hat{V}_{02} \sim \Omega_{DE}$ and $\beta > 0$. All these choices ensure that ψ_0 is a real-valued quantity, condition that holds even for the uncoupled case. Notice that there exists an extra condition coming from the coupling sector that enforces the field amplitude to lie in the domain $\psi_0^2 < \frac{2}{3\alpha}$. However, as ψ_0 is already fixed, this will set rather a plausible range for α values, ensuring thus consistency between free parameters. Finally, the normalized matter density follows from

$$\hat{\rho}_{m,0} = \frac{\Omega_{m,0}}{f_0}, \quad f_0 = (1 + \alpha \hat{X}_0)^n, \quad \hat{X}_0 = -\frac{3}{2} \psi_0^2. \quad (2.22)$$

This means that for given values of the free coupling parameters α and n , the matter density today is fully determined. In absence of coupling, of course, it does not require information of the field amplitude ψ_0 . This setup guarantees that the Friedmann constraint is exactly satisfied at the initial time by construction. To ensure the physical consistency of the numerical evolution, the code continuously monitors the dimensionless Friedmann residual,

$$\Delta_F = \frac{\hat{\mathcal{H}}^2 - a^2(f\hat{\rho}_m + \frac{1}{2}\frac{\chi^2}{a^4} + \hat{V})}{\hat{\mathcal{H}}^2}, \quad (2.23)$$

which remains at the level of machine precision throughout the integration. The physical domain of parameters is restricted to $\lambda > 1/3$, $\hat{V}_0 > \Omega_{\text{DE},0}$, and coupling strengths $|\alpha| \lesssim \mathcal{O}(1)$ with $n \in [-1, 1]$, which are consistent with recent observational constraints [54]. We integrate backwards from today to the emission time, using Radau stiff integrator, ensuring regularity and numerical stability of the solutions.

From now on, we refer to *model 1* as the case characterized by the exponential potential (see Eq. 2.17) together with the coupling function defined in Eq. (2.18), and to *model 2* as the case with the power-law potential (see Eq. 2.17) featuring a weak coupling, as we will adopt small values for the coupling parameters. This classification encompasses the most representative scenarios within this class of vector-like dark energy models and allows us to extract general conclusions.

To characterize the background dynamics, it is useful to introduce the effective equation of state (EoS) w_{eff} and the vector dark energy EoS w_A , which provide a clear diagnostic of

²It means that the background solution will match the Λ CDM solution at the present time. Notice that this can generally be achieved with a non-vanishing, thought small, vector field, leading to a weak coupling to dark matter.

the dominant energy component and its evolution. They are defined as

$$w_{\text{eff}} = \frac{P_T}{\rho_T}, \quad w_A = \frac{P_A}{\rho_A}, \quad (2.24)$$

and can be computed from Eqs. (2.10)–(2.11) for the total fluid, and from Eqs. (2.13)–(2.14) for the vector sector.

Figure 1 displays the evolution of w_{eff} and w_A for the two models under consideration. At an intermediate stage³, both models exhibit small departures from the radiation-like value $w_A = 1/3$, induced by the energy exchange term in the continuity equations. These deviations are more pronounced in *model 1*, where the stronger coupling produces a sharper rise and a visible bump in w_A , whereas in *model 2* the weaker coupling does not produce any observable signature.

As the universe expands and the interaction becomes subdominant, the dynamics of the vector field gradually approach the attractor behavior characteristic of the late-time de Sitter phase. Consequently, both models asymptotically converge to $w_A = -1$, signaling that the vector field *successfully mimics a cosmological constant at late times*. w_{eff} follows the same trend, reflecting the eventual dominance of the dark energy sector over the total energy density. Although both models share the same late-time limit, their distinct early-time behavior may play an important role in determining the magnitude of the gravitational-wave amplitude modulation discussed in the following sections.

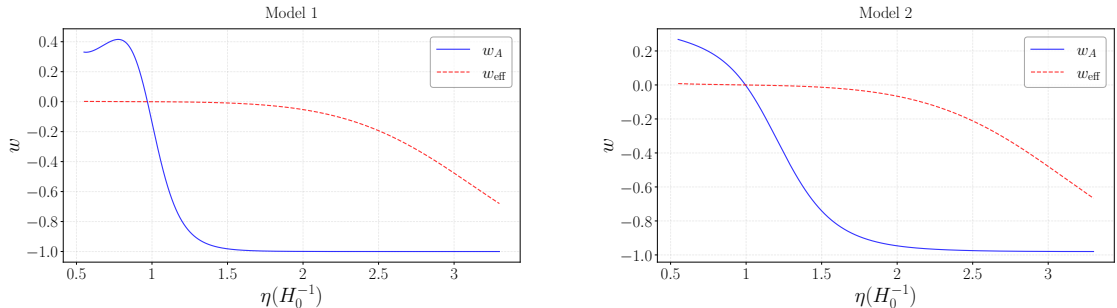


Figure 1. Evolution of the effective EoS w_{eff} and the vector dark energy EoS w_A as a function of conformal time η for *model 1* (strongly coupled exponential potential) in the *left panel* and *model 2* (weakly coupled power-law potential) in the *right panel*. At late times, both models approach the de Sitter solution $w_A = -1$, while at intermediate stage, corresponding to the onset of the evolution, slight differences appear before reaching the radiation-like behavior $w_A = 1/3$. For model 1, this deviation is induced by the strong vector–matter coupling, which produces a sharp rise followed by a small bump. For model 1, we set the parameters $\alpha = 0.65$, $n = -0.3$, $\lambda = 0.34$, and $\hat{V}_{01} = 0.68001$. For model 2, we use $\alpha = -0.09$, $n = -0.009$, $\beta = -0.09$, and $\hat{V}_{02} = 0.690$. For both models we set $\chi_0 = 5 \times 10^{-4}$, which uniquely determines the amplitude ψ_0 via Eqs. (2.20) and (2.21), respectively.

³The emission time considered here corresponds to $z \approx 265$. Since matter–radiation equality occurs at $z \approx 3400$, the Universe is therefore well within the matter-dominated epoch at this stage, which is why we refer to it as an intermediate regime rather than early times, when radiation dominates the energy budget. The choice of such a high redshift is merely illustrative and serves to validate the consistency of the background evolution.

3 Gravitational waves oscillations

We investigate the propagation of GWs in the presence of a background vector field. To this end, we begin by perturbing the spacetime metric as

$$ds^2 = g_{\mu\nu} dx^\mu dx^\nu = (\bar{g}_{\mu\nu} + h_{\mu\nu}) dx^\mu dx^\nu, \quad (3.1)$$

where $\bar{g}_{\mu\nu}$ is the homogeneous and isotropic background metric introduced in Eq. (2.8). In addition, the vector field is perturbed according to

$$A_{a\mu} = \bar{A}_{a\mu} + y_{a\mu}. \quad (3.2)$$

The presence of both the internal index a and the spacetime index μ allows the perturbations $y_{a\mu}$ to couple non-trivially to tensor modes of the metric. In other words, these perturbations support, and can modify, the propagation of helicity-2 or tensor degrees of freedom. From these definitions, the resulting linearized equations for the metric and vector-field perturbations can be found in Appendix A.

Since the background is homogeneous and isotropic, the perturbations of the field equations at linear order are decoupled according to their helicity [55]. The metric radiative degrees of freedom are traceless and transverse, thus we will restrict our study to helicity 2 degrees of freedom. The equation for the metric perturbations can be written in the following form

$$\square_s \delta^{ik} h_{kj}^{\text{TT}} = -2M_{\text{Pl}}^{-2} [\delta K_j^i + \delta M_j^i]^{\text{TT}}, \quad (3.3)$$

where \square_s is the scalar wave operator (see e.g. [56]),

$$\square_s \equiv (-\bar{g})^{-1/2} \partial_\alpha [(-\bar{g})^{-1/2} \bar{g}^{\alpha\beta} \partial_\beta], \quad (3.4)$$

For simplicity, we consider perturbations propagating along the z -direction. Accordingly, the transverse-traceless metric perturbation can then be written as

$$h_{ij}^{\text{TT}} = a(\eta)^2 \begin{bmatrix} h_+ & h_\times & 0 \\ h_\times & -h_+ & 0 \\ 0 & 0 & 0 \end{bmatrix}, \quad (3.5)$$

and analogously the spatial components of the vector-field perturbation take the form

$$y_{ai} = a(\eta) \begin{bmatrix} y_+ & y_\times & 0 \\ y_\times & -y_+ & 0 \\ 0 & 0 & 0 \end{bmatrix}. \quad (3.6)$$

Both h_{ij}^{TT} and y_i^a satisfy the transverse and traceless conditions: $\partial^i h_{ij} = h_i^i = 0$ and $\delta_a^i \partial_i y_j^a = \delta_a^i y_i^a = 0$. Thus, the tensor sector contains four dynamical degrees of freedom corresponding to the $+$ and \times polarization states of the metric and vector fields.

To simplify the equations of motion, it is convenient to redefine the perturbation variables as

$$h_P = \sqrt{2} \hat{h}_P / (a M_{\text{Pl}}), \quad y_P = \hat{y}_P / (\sqrt{2} a), \quad (3.7)$$

with $P = \pm$. After transforming to Fourier space, it is convenient to group the tensor modes in the two-component column vector $\vec{\Phi} = \begin{bmatrix} \tilde{h}_k \\ \tilde{y}_k \end{bmatrix}$. Using the background equations and the

definitions above, the coupled system for tensor perturbations can be written in the compact matrix form:

$$\left(\mathbf{I} \frac{d^2}{d\eta^2} + \mathbf{I}k^2 + \mathbf{f} \frac{d}{d\eta} + \mathbf{M} \right) \vec{\Phi} = 0, \quad (3.8)$$

where \mathbf{I} is the 2×2 matrix identity. The friction matrix is given by

$$\mathbf{f} = \begin{bmatrix} 0 & f_{12} \\ f_{21} & 0 \end{bmatrix} = \begin{bmatrix} 0 & \frac{2\varphi'}{aM_{\text{Pl}}} \\ -\frac{2\varphi'}{aM_{\text{Pl}}} & 0 \end{bmatrix}, \quad (3.9)$$

and the mass matrix reads

$$\mathbf{M} = \begin{bmatrix} m_{11}^2 & m_{12}^2 \\ m_{21}^2 & m_{22}^2 \end{bmatrix} = \begin{bmatrix} \frac{2\varphi^2}{M_{\text{Pl}}^2} \bar{\mu}_A^2 - \mu_H^2 & -\frac{2\varphi a}{M_{\text{Pl}}} \bar{\mu}_A^2 \\ \frac{2\mathcal{H}\varphi'}{aM_{\text{Pl}}} & a^2 \bar{\mu}_A^2 \end{bmatrix}. \quad (3.10)$$

Here we have defined $\mu_H^2 \equiv \frac{2\varphi'^2}{a^2 M_{\text{Pl}}^2} + \mathcal{H}' + \mathcal{H}^2$, which encodes information of the standard friction term and kinetic energy of the vector field. The off-diagonal entries of \mathbf{f} and \mathbf{M} are responsible, respectively, for the damping and oscillatory modulation of amplitude between the metric h and the auxiliary tensor mode y , reflecting their gravitational mixing. To solve the coupled system consistently, we must first solve the background dynamics, which induces an explicit time dependence in the coefficients of Eq. (3.8).

The system cannot be diagonalized in general because \mathbf{f} and \mathbf{M} do not commute, and can not be solved analytically because of the time-dependence coefficients⁴. However, both eigenmodes propagate with the same group velocity, ensuring that the tensor modes remain coherent during propagation.

The matrices \mathbf{f} and \mathbf{M} evolve adiabatically, i.e., their characteristic time is much longer than the typical period of the perturbations. Depending on the wavenumber k , the system admits either a WKB approximation (when k is comparable to the matrix elements) or eikonal approximation (when k is much larger). It is therefore convenient to define a critical wavelength that marks the transition between the WKB and eikonal regimes for the mass term. Since the background scales are determined by the Hubble rate and the field mass is ultra-light ($m \lesssim 10^{-33}$ eV), a critical transition frequency is defined at $f_{\text{crit}} \sim 10^{-18}$ Hz.

3.1 Oscillations of the Waveform

In this subsection, we assess the accuracy of the WKB approximation by comparing it with the full numerical solution of the coupled perturbation system Eq. (3.8). The analysis is performed using the background solutions obtained in the previous section for *model 1* and *model 2*, where the model parameters are fixed to ensure a self-consistent late-time cosmology.

We refer the reader to Ref. [49] for a comprehensive discussion of the WKB treatment of tensor mixing; in particular, Sec. 2.2.1 presents the derivation of the mixing induced by

⁴Given the antisymmetric structure of the friction matrix, the propagation equation can be cast into a compact form via the field redefinition $\vec{\Phi} = \mathbf{S} \vec{\Psi}$, where \mathbf{S} is invertible by construction. The system then reduces to

$$\left(\mathbf{I} \frac{d^2}{d\eta^2} + \mathbf{I}k^2 + \mathbf{M}_{\text{eff}} \right) \vec{\Psi} = 0,$$

with the effective mixing mass, given by $\mathbf{M}_{\text{eff}} = \mathbf{S}^{-1} \mathbf{M} \mathbf{S} - \frac{1}{2} \mathbf{f}' - \frac{1}{4} \mathbf{f}^2$, encapsulates not only the original mass terms but also the effects induced by the friction matrix.

the mass matrix. As in bigravity, the observable modulation of the GW signal is governed by the mixing angle, defined as

$$\tan^2 \theta_g = \frac{m_{12}^2 m_{21}^2}{m_{11}^2 + M^2 \Delta/2}, \quad (3.11)$$

where $M^2 \equiv m_{11}^2 + m_{22}^2$ and $\Delta = \sqrt{1 - 4 \det(\mathbf{M})/M^4} - 1$ follows the notation of Ref. [49]. We evaluate the mixing angle numerically both at emission and at the present epoch in order to quantify its evolution during propagation, finding that

$$\text{model 1:} \quad 0.0503068\pi < \theta_g < 0.496988\pi, \quad (3.12)$$

$$\text{model 2:} \quad 0.486369\pi < \theta_g < 0.499204\pi. \quad (3.13)$$

The interval for *model 1* interestingly overlaps with the region in which oscillatory features in bigravity could, in principle, be detectable by LISA, namely $0.05\pi < \theta_g < 0.45\pi$ [57]. In contrast, for *model 2* the mixing angle is essentially frozen throughout the evolution.

A central aspect of the propagation analysis is the identification of the characteristic oscillation frequency between the tensor modes. This frequency is controlled by the difference of the eigenfrequencies of the system (see e.g., [49]),

$$\delta\theta \simeq \frac{\delta m}{2k} = \sqrt{\mu_A^2 \left(a^2 - 2 \frac{\varphi^2}{M_p^2} \right) + \mu_H^2}, \quad (3.14)$$

where $\delta m \equiv \sqrt{m_{22}^2 - m_{11}^2}$ (see Eq. (3.10) for definitions of m_{ii}^2) quantifies the difference between the eigenmasses of the coupled system. The expression above makes explicit that the oscillation frequency depends directly on the effective mass in the high- k limit. It is convenient to re-express the eigenfrequency in terms of the *mixing mass* m_g . This reads

$$\delta\theta \equiv \frac{m_g^2}{2k} \quad \Rightarrow \quad m_g \sim \mu_A. \quad (3.15)$$

Thus, the modulation oscillates with a characteristic frequency set by the mixing mass, whose magnitude is primarily controlled by the effective mass term in the mass matrix⁵. We can use the fact that the background evolution drives μ_A toward a value of order the present Hubble scale, $\mu_A \sim \mathcal{H}_0$. Consequently,

$$m_g \sim \mu_A \sim \mathcal{H}_0 \approx 10^{-33} \text{eV}, \quad (3.16)$$

which clearly shows that the mixing scale at the order of the present Hubble rate \mathcal{H}_0 —precisely the mass scale expected for a DE scale field. In contrast to earlier studies, this small value of m_g is not a free parameter but is instead fixed by the background solution, which strongly constrains the viable dynamics of the tensor-mixing sector.

Next phenomenological aspect we want to examine is the usual assumption of *time-independent coefficients* for a given wavenumber k in this model. The numerical results show that for $k = 100$ there exists a critical redshift $z \gtrsim 3$ beyond which this assumption no longer holds. Interestingly, this regime approximately overlaps with the expected redshift range of

⁵This follows from the fact that, in the matrix component m_{11}^2 , the term μ_A^2 dominates over μ_H^2 , while $|2\varphi^2/(a^2 M_p^2)| \ll 1$ throughout the entire evolution from emission to today, as verified numerically.

standard sirens from supermassive black hole mergers, $z \sim \mathcal{O}(1 - 10)$, which is significantly larger than the typical LIGO/Virgo sources ($z \ll 1$).

As a representative example for each model, Fig. 2 shows the evolution of the auxiliary mode y (left panels) and the GW amplitude $|h|^2$ (right panels) for *model 1* (top) and *model 2* (bottom). We display three cases of interest: the full numerical solution, the WKB approximation, and the solution obtained by neglecting the friction term. From these results it is clear that the WKB approximation *overestimates* the growth of the dark auxiliary tensor mode (left panels), which in turn leads to an artificial suppression of the GW amplitude through the periodic conversion of h into y (right panels).

Increasing the wavenumber to $k = 500$ produces a comparable net damping of the GW signal, albeit with faster oscillations. For this reason, it is not particularly informative to display even higher- k results in this section. As expected for a secular effect, the discrepancy between the WKB and numerical solutions becomes increasingly significant for earlier emission times.

One may argue that the friction term \mathbf{f} could be safely neglected, since its contribution is subdominant at the present epoch. However, retaining this term is essential for higher-redshift emissions, where its magnitude grows substantially. In general we find that $\mathbf{f} \sim \rho_{\text{Kin}}^{1/2}/a(\eta)$, with $\rho_{\text{Kin}} \sim \varphi'^2/a^4$. Thus, at the emission time ρ_{Kin} may be several orders of magnitude smaller than the present critical density, $\rho_{\text{crit},0}$, but still large enough to affect the early-time dynamics. Moreover, while the component f_{12} increases sharply towards the past, f_{21} exhibits the opposite trend (see Eq. (3.9) for definitions of f_{ii}) . This opposite evolution is responsible for the small amplitude attained by the vector perturbation y (see left panel of Fig. 2). Despite this, the corresponding impact on the GW amplitude remains negligible (right panel), as the suppression generated by the friction term is efficiently counteracted by the background scaling. This behavior explains the very small amplitude associated with the tensor mode y , while the GW amplitude remains practically unaffected.

During the evolution, both effective masses μ_A^2 and μ_H^2 may undergo sign changes. This occurs most notably in *model 2*, where μ_H^2 switches sign and thus reverses the direction of the mixing-induced energy exchange between the tensor modes. In the WKB treatment, this sign flip momentarily transforms the mixing from a damping regime, where mixing extracts energy from h , to an enhancing regime where the auxiliary mode injects energy back into the GW sector. However, this behavior is *not* genuinely captured by the full numerical solution: the oscillation pattern remains monotonic, and no physical reversal of the amplitude transfer is observed. This indicates that the apparent sign-flip effect is an artefact of the WKB approximation and does not correspond to an actual dynamical feature of the system.

The next question we wish to address is whether these effects are potentially observable within the frequency band of current and future GW detectors. This step is essential in order to establish a realistic physical scenario and to discard claims that may arise from regimes that are not experimentally accessible.

3.2 A Realistic Scenario

We inferred in the previous section that the modulation of the GW amplitude becomes more pronounced for high-redshift astrophysical sources. However, it remains unclear whether such effects can leave any appreciable imprint on the observable GW strain measured by ground-based or space-based interferometers. To address this question, we must translate our theoretical predictions into the characteristic frequency ranges of existing detectors: LIGO/Virgo operates at $f \sim 10$ Hz, whereas LISA is sensitive to much lower frequencies,

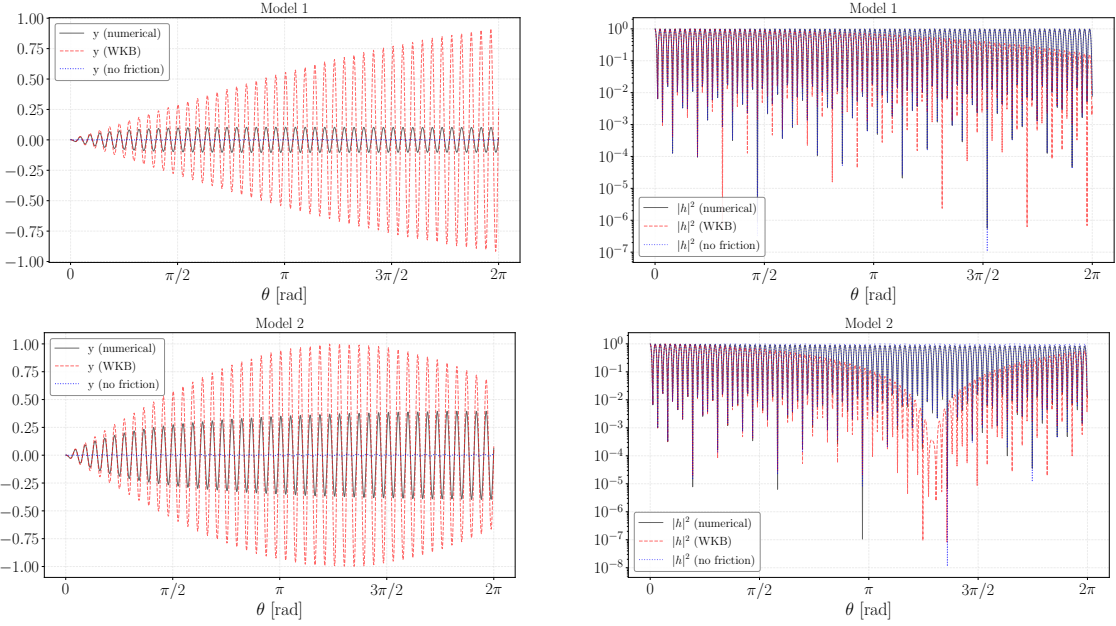


Figure 2. Evolution of the auxiliary tensor mode y (left) and the GW amplitude $|h|^2$ (right) for *model 1* (top) and *model 2* (bottom). Here, $\theta = 2\pi(\eta - \eta_e/\Delta\eta)$, with $\Delta\eta = \eta_0 - \eta_e$. We show the full numerical solution, the WKB approximation, and the result obtained by neglecting the friction term. The WKB method overestimates the growth of y , leading to an artificial suppression of the GW amplitude, while the full solution exhibits only mild damping. The no inclusion of the friction term prevents significant growth of y , but keeping the GW amplitude essentially unchanged. In *model 2*, the sign flip of μ_H^2 produces an apparent reversal of mixing in the WKB approximation, but this effect does not occur in the numerical evolution, confirming that this feature is a methodological artefact. We have taken the following initial conditions at the emission time: $h_0 = 1$, $y_0 = 0$, $h'_0 = 10^{-3}$ and $y'_0 = 10^{-3}$ and $k = 100$.

$f \sim 10^{-3}$ Hz, each within their corresponding observational bands. The large LIGO/Virgo frequencies allow us to employ, in addition to the WKB treatment, the high- k limit⁶.

The impact of a mass-type mixing on the observed GW amplitude can be encoded in a frequency and redshift-dependent *transfer function*. Assuming that the effective mixing angle θ_g and mixing mass m_g vary slowly along the line of sight, the ratio between the observed strain and the GR expectation is given by [49, 57]

$$\frac{|h(z, k)|}{|h_{\text{GR}}|} = \cos^2 \theta_g \left[1 + \tan^4 \theta_g + 2 \tan^2 \theta_g \cos \left(\int_0^z \frac{m_g^2}{2k} \frac{dz'}{H(z')} \right) \right]^{1/2}, \quad (3.17)$$

which captures the leading oscillatory corrections to the waveform. The phase is proportional to m_g^2/k , and therefore highly suppressed at large frequencies. The transfer function depends on θ_g , m_g , the source redshift, and the background expansion rate.

In what follows, we evaluate the integral in Eq. (3.17) using the self-consistent Hubble rate $H(z)$ obtained from our Multi-Proca background solutions, rather than imposing a fiducial Λ CDM history. We expect, however, to obtain a very minor correction, that for

⁶In such a regime one has $k = \frac{2\pi f}{H_0} \sim 10^{20}$, which are far too large to be implemented in the numerical analysis of the previous section. This is precisely why several studies adopt a more moderate value, typically $k \sim 10^3$, when examining the dynamics of mixed helicity-2 modes (see e.g., [49, 58]).

this estimation is not crucial. More importantly, in order to have an observable effect, the ratio m_g^2/k must be of order H_0 . Considering that $m_g \approx \mu_A(z)a(z)$, with $a(z) = \frac{1}{(1+z)}$, the oscillatory phase that controls the modulation in the transfer function (see Eq. (3.17)) can be written as

$$\Phi(z, f) \equiv \frac{\mu_A^2}{2k} I(z), \quad I(z) \equiv \int_0^z \frac{dz'}{(1+z')^2 H(z')}, \quad (3.18)$$

where we have assumed that μ_A does not vary rapidly so that it can be taken outside the integral. This is essentially true for low- z sources. The condition for a sizable oscillatory effect is $\Phi \gtrsim 1$. Rearranging,

$$\Phi \sim 1 \implies f \sim \frac{I(z) \mu_A^2}{4\pi}. \quad (3.19)$$

To obtain numerical estimates, we take $H_0 \simeq 2.2 \times 10^{-18} \text{ s}^{-1}$ and compute numerically $I(z)$. This is done for *model 1* for the sake of example. The result shows that $I(z)$ saturates quickly with redshift: most of its contribution comes from the low- z region ($z \lesssim 1$) it being of order $1/H_0$, and for $z \gtrsim 10$ one finds $I(z) \sim 10^{17} \text{ s}$ (i.e., few $\times 1/H_0$). Inserting this into Eq. (3.19) gives

$$f_{\text{req}} \sim 10^{-18} \text{ Hz}, \quad (3.20)$$

an astronomically small value. This estimate shows that, for $m_g \sim 10^{-33} \text{ eV}$, the phase Φ is completely negligible across the LIGO/LISA frequency bands and for any realistic source redshift: even at the lowest PTA frequencies, Φ remains many orders of magnitude below unity. Detectable oscillatory signatures of the type encoded in Eq. (3.17) would therefore require either much larger effective mixing masses (well above the dark-energy scale) or access to unrealistically low GW frequencies (well below the PTA range).

A crucial point in this analysis is that we have so far treated μ_A as a fixed parameter, even though it is intrinsically time-dependent. This approximation is adequate at low redshift, where the variation of $\mu_A(z)$ is mild. However, at higher redshift the effective mass may evolve significantly and can reach values much larger than its present-day value. Therefore, a consistent assessment of the accumulated oscillatory phase in Eq. (3.17) must take into account the redshift evolution of μ_A . Before turning to the numerical results, it is useful to examine a few limiting cases.

In the low-redshift limit ($z \ll 1$), the integrand in the cumulative phase becomes nearly constant to leading order, since $\mu_A \rightarrow H_0$ and $H(z) \rightarrow H_0$. Analytically this gives $\Phi(z) \approx \frac{H_0 z}{4\pi f}$, implying a linear but extremely suppressed growth at small z , consistent with the rapid numerical decay of the phase as $z \rightarrow 0$. At high redshift, where $\mu_A^2(z)$ grows only mildly compared to the strong $(1+z)^2$ suppression, the integral saturates and remains far below unity across a wide frequency range. Numerically, we find that even up to $z = 200$ (unrealistic redshift sources), the cumulative phase remains $\Phi \ll 1$ for representative frequencies spanning the PTA, LISA, and ground-based bands, with typical values $\Phi_{\text{max}} \simeq 10^{-7}$ at $f = 10^{-9} \text{ Hz}$, $\Phi_{\text{max}} \simeq 10^{-13}$ at $f = 10^{-3} \text{ Hz}$, and $\Phi_{\text{max}} \simeq 10^{-18}$ at $f = 10^2 \text{ Hz}$.

These results confirm that, for late-universe propagation, mixing-induced phase accumulation is inefficient at both low and high redshift, making observable oscillatory effects highly suppressed. These findings are summarized in Fig. 3, where the cumulative phase shift $\Phi(z; f)$ as a function of redshift for representative GW frequency bands (PTA, LISA, and LIGO/Virgo) is computed numerically, using the interpolated functions $\mu_A^2(z)$ and $H(z)$ from the background solution.

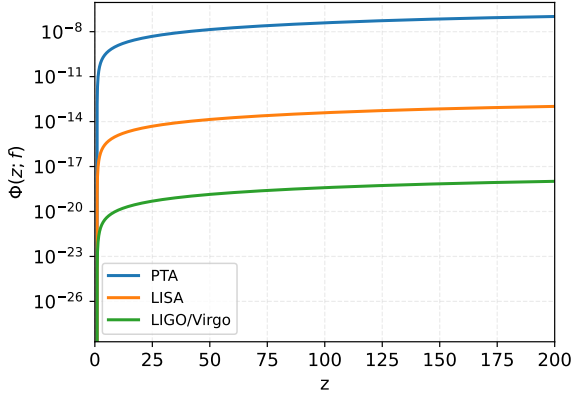


Figure 3. Cumulative phase shift $\Phi(z; f)$ as a function of redshift for representative GW frequency bands (PTA: $f = 10^{-9}$ Hz, LISA: $f = 10^{-3}$ Hz, and LIGO/Virgo: $f = 10^2$ Hz). The phase is computed using the interpolated functions $\mu_A^2(z)$ and $H(z)$ for the *model 1*. At low redshift the phase grows linearly but remains extremely small, while at high redshift the integral saturates, producing a plateau consistent with the weak redshift dependence of μ_A . In all cases, the accumulated phase remains far below unity over the full range $z \leq 200$.

While oscillation-induced amplitude are intrinsically suppressed for astrophysical GW sources in these models, a particularly promising avenue for future work is the study of the stochastic GW background propagating through a dynamically evolving Multi-Proca sector in the early Universe, where the vector fields behave effectively as dark radiation. In the post-inflationary era, the vector amplitude can be many orders of magnitude larger than today, potentially allowing for significant amplification or suppression of the primordial tensor spectrum. Remarkably, even a relatively small energy density in a triplet of canonical $U(1)$ vector fields can leave observable imprints in the polarization B-mode pattern of the cosmic microwave background (CMB) [59, 60]. This suggests that early-universe Multi-Proca dynamics may produce distinctive signatures accessible to next-generation probes of primordial gravitational waves, including the South Pole Telescope [61], POLARBEAR [62], and the Atacama Cosmology Telescope [63].

4 Conclusions

In this work, we have investigated GW oscillations induced by the mixing between tensor metric perturbations and multiple vector fields, with particular emphasis on the class of Multi-Proca DE models. Although previous studies suggested that such *dark spin-1 sectors* may imprint observable signatures on GW propagation, such as modulations of the waveform [49], it remained unclear whether the proposed theoretical framework can simultaneously sustain a consistent cosmological background. Without this requirement, any predicted observational effect would lack physical reliability.

A key distinction of our analysis is that we neither impose a Λ CDM background nor rely on phenomenological parameterizations for the matrix coefficients. Instead, we solve self-consistently for the cosmological background, which in turn fixes the free parameters of the vector sector. Only with this fully consistent setup can the predicted modulation of the GW amplitude be meaningfully and robustly quantified.

We have shown that GW amplitude modulation does occur in Multi-Proca-like dark energy models, exhibiting clear and well-defined oscillatory patterns in the waveform. These effects are more prominent for high-redshift sources, where neither the WKB approximation nor the frictionless limit fully captures the dynamics in the regime of low frequencies. Nonetheless, for low-redshift sources and high-frequencies signals, such as those relevant for LIGO/Virgo, these approximations remain fully adequate.

The central result of this study is that the modulation amplitude is severely constrained by the extremely small value of the mixing mass, $m_g \sim \mu_A \sim \mathcal{H}_0$, which is a direct consequence of enforcing a self-consistent background solution. This ultra-light mass regime coincides with that found in bigravity [57], where the oscillatory factor m_g^2/k cannot produce an $\mathcal{O}(1)$ modulation of the observed strain for any realistic detector frequency or source redshift.

Our results are also consistent with those found for the *gauge-essence* model, an SU(2) gauge-field dark energy scenario, where the suppression of the GW amplitude remains far below the sub-percent level even for sources located at very high redshift [53].

We therefore conclude that, if a modulation of the GW amplitude were ever detected by current ground-based interferometers or future space-based detectors, such an effect *cannot* be attributed to multiple vector fields, either in Multi-Proca or SU(2) gauge-field realizations, within the class of vector-like dark energy models considered in this work. It remains an open question whether the inclusion of non-minimal couplings to gravity, capable of supporting self-accelerated solutions (see e.g., [40, 64]), could modify this conclusion by allowing for a different mixing mass. Addressing this possibility lies beyond the scope of the present work and warrants a dedicated investigation.

Despite this pessimistic outlook for direct modulation effects, our analysis highlights an important opportunity: ultra-light vector fields may still leave distinctive imprints on the stochastic GW background at low frequencies [65]. In the early Universe, where the vector sector behaves effectively as dark radiation, the amplitude of the auxiliary tensor mode can be significantly larger, potentially leading to appreciable amplification or suppression of primordial tensor modes. This suggests that Multi-Proca dynamics may offer promising avenue for next-generation probes of primordial GWs.

A Tensor perturbations

This Appendix details the derivation of the equations governing perturbation dynamics. We recall that barred quantities refer to those defined with respect to the background variables. The perturbed field equations take the following form:

$$\delta G^\mu_\nu = M_{\text{Pl}}^{-2} \delta T^\mu_\nu = M_{\text{Pl}}^{-2} (\delta K^\mu_\nu + \delta M^\mu_\nu), \quad (\text{A.1})$$

and

$$\begin{aligned} \bar{\nabla}_\alpha \delta F_a^\alpha_\nu - \frac{1}{2} \bar{F}_{a\nu}^\alpha \bar{\nabla}_\alpha h^\beta_\beta + h^{\alpha\beta} \bar{\nabla}_\beta \bar{F}_{a\nu\alpha} + \bar{F}_{a\nu}^\alpha \bar{\nabla}_\beta h_\alpha^\beta + \bar{F}_a^{\alpha\beta} \bar{\nabla}_\beta h_{\nu\alpha} - 2y_{a\nu} V_{,\tilde{X}} \\ - 4\bar{A}_{a\nu} \bar{A}^{b\alpha} y_{b\alpha} V_{,\tilde{X}\tilde{X}} + 2\bar{A}_{a\nu} \bar{A}_b^\beta \bar{A}^{b\alpha} h_{\alpha\beta} V_{,\tilde{X}\tilde{X}} + \bar{A}_{a\nu} \delta(f_{,X} \mathcal{L}_{\tilde{m}}) + y_{a\nu} \bar{f}_{,X} \bar{\mathcal{L}}_{\tilde{m}} = 0, \end{aligned} \quad (\text{A.2})$$

The perturbation of the mixed Einstein tensor is given by

$$\begin{aligned} \delta G^\mu_\nu = -\bar{G}_\nu^\alpha h^\mu_\alpha + \frac{1}{2} \delta^\mu_\nu h^{\alpha\beta} \bar{R}_{\alpha\beta} - \frac{1}{2} h^\mu_\nu \bar{R} - \frac{1}{2} \bar{\nabla}_\alpha \bar{\nabla}^\alpha h^\mu_\nu + \frac{1}{2} \bar{\nabla}_\alpha \bar{\nabla}^\mu h_\nu^\alpha + \frac{1}{2} \bar{\nabla}_\alpha \bar{\nabla}_\nu h^{\mu\alpha} \\ - \frac{1}{2} \delta^\mu_\nu \bar{\nabla}_\beta \bar{\nabla}_\alpha h^{\alpha\beta} + \frac{1}{2} \delta^\mu_\nu \bar{\nabla}_\beta \bar{\nabla}^\beta h_\alpha^\alpha - \frac{1}{2} \bar{\nabla}^\mu \bar{\nabla}_\nu h_\alpha^\alpha, \end{aligned} \quad (\text{A.3})$$

and the perturbation of the Faraday tensor is

$$\delta F^a{}_{\mu\nu} = \bar{\nabla}_\mu y^a{}_\nu - \bar{\nabla}_\nu y^a{}_\mu, \quad (\text{A.4})$$

The tensors constituting the perturbed energy-momentum tensor are:

$$\begin{aligned} \delta K^\mu{}_\nu = & -\bar{F}_{a\nu}{}^\beta \bar{F}^{a\mu\alpha} h_{\alpha\beta} + \bar{F}_{a\alpha}{}^\beta \bar{F}^a{}_\nu{}^\alpha h^\mu{}_\beta + \bar{F}^a{}_\nu{}^\alpha \delta F_a{}^\mu{}_\alpha + \bar{F}^{a\mu\alpha} \delta F_{a\nu\alpha} + \frac{1}{2} \delta^\mu{}_\nu \bar{F}_{a\alpha}{}^\lambda \bar{F}^{a\alpha\beta} h_{\beta\lambda} \\ & - \frac{1}{2} \delta^\mu{}_\nu \bar{F}^{a\alpha\beta} \delta F_{a\alpha\beta} + 2\bar{A}^a{}_\nu y_a{}^\mu V_{,\tilde{X}} + 2\bar{A}^{a\mu} y_{a\nu} V_{,\tilde{X}} - 2\bar{A}^{a\alpha} y_{a\alpha} \delta^\mu{}_\nu V_{,\tilde{X}} + \bar{A}_a{}^\beta \bar{A}^{a\alpha} \delta^\mu{}_\nu h_{\alpha\beta} V_{,\tilde{X}} \\ & - 2\bar{A}_a{}^\alpha \bar{A}^a{}_\nu h^\mu{}_\alpha V_{,\tilde{X}} + 4\bar{A}_{a\nu} \bar{A}^{a\mu} \bar{A}^{b\alpha} y_{b\alpha} V_{,\tilde{X}\tilde{X}} - 2\bar{A}_{a\nu} \bar{A}^{a\mu} \bar{A}_b{}^\beta \bar{A}^{b\alpha} h_{\alpha\beta} V_{,\tilde{X}\tilde{X}}, \quad (\text{A.5}) \end{aligned}$$

$$\begin{aligned} \delta M^\mu{}_\nu = & \bar{\mathcal{M}}^\mu{}_\nu \delta f + \bar{f} \delta \mathcal{M}^\mu{}_\nu + \delta(f_{,X} \mathcal{L}_{\tilde{m}}) \bar{A}_a{}^i \bar{A}^a{}_j \\ & + \bar{f}_{,X} \bar{\mathcal{L}}_{\tilde{m}} (\bar{A}^a{}_\nu y_a{}^\mu + \bar{A}^{a\mu} y_{a\nu} - \bar{A}_a{}^\alpha \bar{A}^a{}_\nu h^\mu{}_\alpha), \quad (\text{A.6}) \end{aligned}$$

where $\delta(f_{,X} \mathcal{L}_{\tilde{m}})$ can be expressed in terms of the following variables:

$$\delta f = f_{,X} \delta X, \quad \delta f_{,X} = f_{,XX} \delta X, \quad (\text{A.7})$$

$$\delta X = \frac{1}{2} \bar{A}^{a\mu} \bar{A}_a{}^\nu h_{\mu\nu} - A^{a\mu} y_{a\mu}, \quad (\text{A.8})$$

$$\delta \mathcal{L}_{\tilde{m}} = \frac{1}{2} (\bar{\mathcal{M}}^{\mu\nu} h_{\mu\nu} - \bar{\mathcal{L}}_{\tilde{m}} h^\mu{}_\mu). \quad (\text{A.9})$$

Acknowledgments

We thank Meng-Xiang for useful correspondence and for kindly providing Python notebooks for generating modified gravitational-wave waveforms.

References

- [1] A. Einstein, *Über Gravitationswellen, Sitzungsber. Preuss. Akad. Wiss. Berlin (Math. Phys.)* **1918** (1918) 154.
- [2] R.A. Hulse and J.H. Taylor, *Discovery of a pulsar in a binary system, Astrophys. J. Lett.* **195** (1975) L51.
- [3] J.M. Weisberg and J.H. Taylor, *Gravitational Radiation From an Orbiting Pulsar, Gen. Rel. Grav.* **13** (1981) 1.
- [4] J.H. Taylor and J.M. Weisberg, *A new test of general relativity: Gravitational radiation and the binary pulsar PS R 1913+16, Astrophys. J.* **253** (1982) 908.
- [5] LIGO SCIENTIFIC, VIRGO collaboration, *Observation of Gravitational Waves from a Binary Black Hole Merger, Phys. Rev. Lett.* **116** (2016) 061102 [[1602.03837](#)].
- [6] L. Lombriser and A. Taylor, *Breaking a Dark Degeneracy with Gravitational Waves, JCAP* **03** (2016) 031 [[1509.08458](#)].
- [7] K. Koyama, *Cosmological Tests of Modified Gravity, Rept. Prog. Phys.* **79** (2016) 046902 [[1504.04623](#)].
- [8] J.M. Ezquiaga and M. Zumalacárregui, *Dark Energy After GW170817: Dead Ends and the Road Ahead, Phys. Rev. Lett.* **119** (2017) 251304 [[1710.05901](#)].
- [9] T. Baker, E. Bellini, P.G. Ferreira, M. Lagos, J. Noller and I. Sawicki, *Strong constraints on cosmological gravity from GW170817 and GRB 170817A, Phys. Rev. Lett.* **119** (2017) 251301 [[1710.06394](#)].

[10] A. Nishizawa, *Generalized framework for testing gravity with gravitational-wave propagation. I. Formulation*, *Phys. Rev. D* **97** (2018) 104037 [[1710.04825](#)].

[11] P.J.E. Peebles and B. Ratra, *Cosmology with a Time Variable Cosmological Constant*, *Astrophys. J. Lett.* **325** (1988) L17.

[12] S. Weinberg, *The Cosmological Constant Problem*, *Rev. Mod. Phys.* **61** (1989) 1.

[13] L. Amendola and S. Tsujikawa, *Dark Energy*, Cambridge University Press (2015).

[14] DESI collaboration, *Extended Dark Energy analysis using DESI DR2 BAO measurements*, [2503.14743](#).

[15] PLANCK collaboration, *Planck 2018 results. VI. Cosmological parameters*, *Astron. Astrophys.* **641** (2020) A6 [[1807.06209](#)].

[16] D. Scolnic et al., *The Pantheon+ Analysis: The Full Data Set and Light-curve Release*, *Astrophys. J.* **938** (2022) 113 [[2112.03863](#)].

[17] D. Brout et al., *The Pantheon+ Analysis: Cosmological Constraints*, *Astrophys. J.* **938** (2022) 110 [[2202.04077](#)].

[18] DES collaboration, *The Dark Energy Survey: Cosmology Results with ~ 1500 New High-redshift Type Ia Supernovae Using the Full 5 yr Data Set*, *Astrophys. J. Lett.* **973** (2024) L14 [[2401.02929](#)].

[19] DESI collaboration, *DESI DR2 Results II: Measurements of Baryon Acoustic Oscillations and Cosmological Constraints*, [2503.14738](#).

[20] A.G. Riess et al., *A Comprehensive Measurement of the Local Value of the Hubble Constant with $1 \text{ km s}^{-1} \text{ Mpc}^{-1}$ Uncertainty from the Hubble Space Telescope and the SH0ES Team*, *Astrophys. J. Lett.* **934** (2022) L7 [[2112.04510](#)].

[21] L. Knox and M. Millea, *Hubble constant hunter’s guide*, *Phys. Rev. D* **101** (2020) 043533 [[1908.03663](#)].

[22] E. Macaulay, I.K. Wehus and H.K. Eriksen, *Lower Growth Rate from Recent Redshift Space Distortion Measurements than Expected from Planck*, *Phys. Rev. Lett.* **111** (2013) 161301 [[1303.6583](#)].

[23] R.A. Battye, T. Charnock and A. Moss, *Tension between the power spectrum of density perturbations measured on large and small scales*, *Phys. Rev. D* **91** (2015) 103508 [[1409.2769](#)].

[24] BOSS collaboration, *The clustering of galaxies in the completed SDSS-III Baryon Oscillation Spectroscopic Survey: cosmological analysis of the DR12 galaxy sample*, *Mon. Not. Roy. Astron. Soc.* **470** (2017) 2617 [[1607.03155](#)].

[25] DES collaboration, *Dark Energy Survey year 1 results: Cosmological constraints from galaxy clustering and weak lensing*, *Phys. Rev. D* **98** (2018) 043526 [[1708.01530](#)].

[26] B. Ratra and P.J.E. Peebles, *Cosmological Consequences of a Rolling Homogeneous Scalar Field*, *Phys. Rev. D* **37** (1988) 3406.

[27] C. Wetterich, *Cosmology and the Fate of Dilatation Symmetry*, *Nucl. Phys. B* **302** (1988) 668 [[1711.03844](#)].

[28] R.R. Caldwell, R. Dave and P.J. Steinhardt, *Cosmological imprint of an energy component with general equation of state*, *Phys. Rev. Lett.* **80** (1998) 1582 [[astro-ph/9708069](#)].

[29] T. Koivisto and D.F. Mota, *Accelerating Cosmologies with an Anisotropic Equation of State*, *Astrophys. J.* **679** (2008) 1 [[0707.0279](#)].

[30] T. Koivisto and D.F. Mota, *Vector Field Models of Inflation and Dark Energy*, *JCAP* **08** (2008) 021 [[0805.4229](#)].

[31] A. Mehrabi, A. Maleknejad and V. Kamali, *Gaugessence: a dark energy model with early time radiation-like equation of state*, *Astrophys. Space Sci.* **362** (2017) 53 [[1510.00838](#)].

[32] A. De Felice, L. Heisenberg, R. Kase, S. Mukohyama, S. Tsujikawa and Y.-l. Zhang, *Cosmology in generalized Proca theories*, *JCAP* **06** (2016) 048 [[1603.05806](#)].

[33] Y. Rodríguez and A.A. Navarro, *Non-Abelian S-term dark energy and inflation*, *Phys. Dark Univ.* **19** (2018) 129 [[1711.01935](#)].

[34] L.G. Gómez and Y. Rodríguez, *Stability Conditions in the Generalized $SU(2)$ Proca Theory*, *Phys. Rev. D* **100** (2019) 084048 [[1907.07961](#)].

[35] J.B. Orjuela-Quintana, M. Alvarez, C.A. Valenzuela-Toledo and Y. Rodriguez, *Anisotropic Einstein Yang-Mills Higgs Dark Energy*, *JCAP* **10** (2020) 019 [[2006.14016](#)].

[36] C. de Rham, S. Garcia-Saenz, L. Heisenberg and V. Pozsgay, *Cosmology of Extended Proca-Nuevo*, *JCAP* **03** (2022) 053 [[2110.14327](#)].

[37] G. Gómez, *Conformally and disformally coupled vector field models of dark energy*, *Phys. Rev. D* **107** (2023) 123535 [[2202.07027](#)].

[38] W. Cardona, J.L. Palacios-Córdoba and C.A. Valenzuela-Toledo, *Scrutinizing coupled vector dark energy in light of data*, *JCAP* **04** (2024) 016 [[2310.13877](#)].

[39] M.C. Pookkillath and K. Koyama, *Theory of interacting vector dark energy and fluid*, *JCAP* **10** (2024) 105 [[2405.06565](#)].

[40] S. Garcia-Serna, J.B. Orjuela-Quintana, Y. Rodriguez, G. Gomez and C.A. Valenzuela-Toledo, *Dynamical shortcomings in the Generalized $SU(2)$ Proca theory: challenges for cosmic acceleration*, *JCAP* **07** (2025) 037 [[2501.17280](#)].

[41] C. Armendariz-Picon, *Could dark energy be vector-like?*, *JCAP* **07** (2004) 007 [[astro-ph/0405267](#)].

[42] T.S. Koivisto and N.J. Nunes, *Coupled three-form dark energy*, *Phys. Rev. D* **88** (2013) 123512 [[1212.2541](#)].

[43] K. Yamamoto, M.-a. Watanabe and J. Soda, *Inflation with Multi-Vector-Hair: The Fate of Anisotropy*, *Class. Quant. Grav.* **29** (2012) 145008 [[1201.5309](#)].

[44] L.G. Gomez and Y. Rodriguez, *Coupled multi-Proca vector dark energy*, *Phys. Dark Univ.* **31** (2021) 100759 [[2004.06466](#)].

[45] C. Rodriguez-Benites, M. Gonzalez-Espinoza, G. Otalora and M. Alva-Morales, *Revisiting the dynamics of interacting vector-like dark energy*, *Eur. Phys. J. C* **84** (2024) 276 [[2311.02397](#)].

[46] J. Beltran Jimenez and L. Heisenberg, *Generalized multi-Proca fields*, *Phys. Lett. B* **770** (2017) 16 [[1610.08960](#)].

[47] M. Gertsenshtein, *Wave resonance of light and gravitational waves*, *Journal of Experimental and Theoretical Physics* **14** (1960) 113.

[48] R.R. Caldwell, C. Devulder and N.A. Maksimova, *Gravitational wave-Gauge field oscillations*, *Phys. Rev. D* **94** (2016) 063005 [[1604.08939](#)].

[49] J. Beltrán Jiménez, J.M. Ezquiaga and L. Heisenberg, *Probing cosmological fields with gravitational wave oscillations*, *JCAP* **04** (2020) 027 [[1912.06104](#)].

[50] K. Max, M. Platscher and J. Smirnov, *Gravitational Wave Oscillations in Bigravity*, *Phys. Rev. Lett.* **119** (2017) 111101 [[1703.07785](#)].

[51] P. Brax, A.-C. Davis and J. Noller, *Gravitational Waves in Doubly Coupled Bigravity*, *Phys. Rev. D* **96** (2017) 023518 [[1703.08016](#)].

[52] J.M. Ezquiaga, W. Hu, M. Lagos and M.-X. Lin, *Gravitational wave propagation beyond general relativity: waveform distortions and echoes*, *JCAP* **11** (2021) 048 [[2108.10872](#)].

[53] R.R. Caldwell and C. Devulder, *Gravitational Wave Opacity from Gauge Field Dark Energy*, *Phys. Rev. D* **100** (2019) 103510 [[1802.07371](#)].

[54] C.S.C.M. Coelho, A.L.Y. Gschrey and C.J.A.P. Martins, *Observational constraints on vectorlike dark energy*, *Phys. Rev. D* **111** (2025) 043543 [[2502.04828](#)].

[55] J.M. Bardeen, *Gauge Invariant Cosmological Perturbations*, *Phys. Rev. D* **22** (1980) 1882.

[56] K.S. Thorne and S.J. Kovacs, *The generation of gravitational waves. I. Weak-field sources.*, *Astrophys. J.* **200** (1975) 245.

[57] LISA COSMOLOGY WORKING GROUP collaboration, *Testing modified gravity at cosmological distances with LISA standard sirens*, *JCAP* **07** (2019) 024 [[1906.01593](#)].

[58] M. de Cesare, M. Sakellariadou and B. Sutton, *Multiple-scale analysis of modified gravitational-wave propagation*, *JCAP* **11** (2025) 071 [[2507.23184](#)].

[59] A.J. Tishue and R.R. Caldwell, *Relic cosmological vector fields and inflationary gravitational waves*, *Phys. Rev. D* **104** (2021) 063531 [[2105.08073](#)].

[60] A.J. Tishue and R.R. Caldwell, *Dark energy with a triplet of classical $U(1)$ fields*, *Phys. Rev. D* **107** (2023) 043514 [[2208.11129](#)].

[61] SPT-3G collaboration, *Measurements of the E-mode polarization and temperature-E-mode correlation of the CMB from SPT-3G 2018 data*, *Phys. Rev. D* **104** (2021) 022003 [[2101.01684](#)].

[62] POLARBEAR collaboration, *A Measurement of the CMB E-mode Angular Power Spectrum at Subdegree Scales from 670 Square Degrees of POLARBEAR Data*, *Astrophys. J.* **904** (2020) 65 [[2005.06168](#)].

[63] ACT collaboration, *The Atacama Cosmology Telescope: B-mode delensing with DR6 data and external tracers of large-scale structure*, [2511.21949](#).

[64] A. Gallego Cadavid, Y. Rodriguez and L.G. Gómez, *Generalized $SU(2)$ Proca theory reconstructed and beyond*, *Phys. Rev. D* **102** (2020) 104066 [[2009.03241](#)].

[65] A. Marriott-Best, M. Peloso and G. Tasinato, *New gravitational wave probe of vector dark matter*, *Phys. Rev. D* **111** (2025) 103511 [[2502.13116](#)].